RSC Advances

ROYAL SOCIETY OF CHEMISTRY

www.rsc.org/advances

Potential apoptosis inducing agents based on a new benzimidazole Schiff base ligand and its dicopper(II) complex

Anup Paul,[a] Rakesh Kumar Gupta,[a] Mrigendra Dubey,[a] Gunjan Sharma,[b] Biplab Koch,[b] Geeta Hundal,[c] Maninderjeet Singh Hundal,[c] and Daya Shankar Pandey*[a]

[a]Departments of Chemistry and [b]Zoology, Faculty of Science, Banaras Hindu University, Varanasi - 221 005 (U.P.) India

[c]Department of Chemistry, Guru Nanak Dev University, Amritsar - 143005 (Punjab), India

The synthesis, characterization and antiproliferative activity of a new benzimidazole based Schiff base 2-(1-methyl-1H-benzimidazol-2-yl)phenyl)imino)methyl)phenol (**HL**) and its dicopper(II) complex $[(Cu(\mathbf{L})NO_3)_2]$ (**CuL**) has been described. DNA/protein binding studies have been investigated by various physicochemical techniques. Molecular docking studies have also been carried out to understand the mode of interaction of **HL** and **CuL** towards DNA/BSA. Further, cytotoxicity of the synthesised compounds have been investigated on MCF-7 cell line and morphological assessment analysed by FACS and AO/EB fluorescence staining techniques.

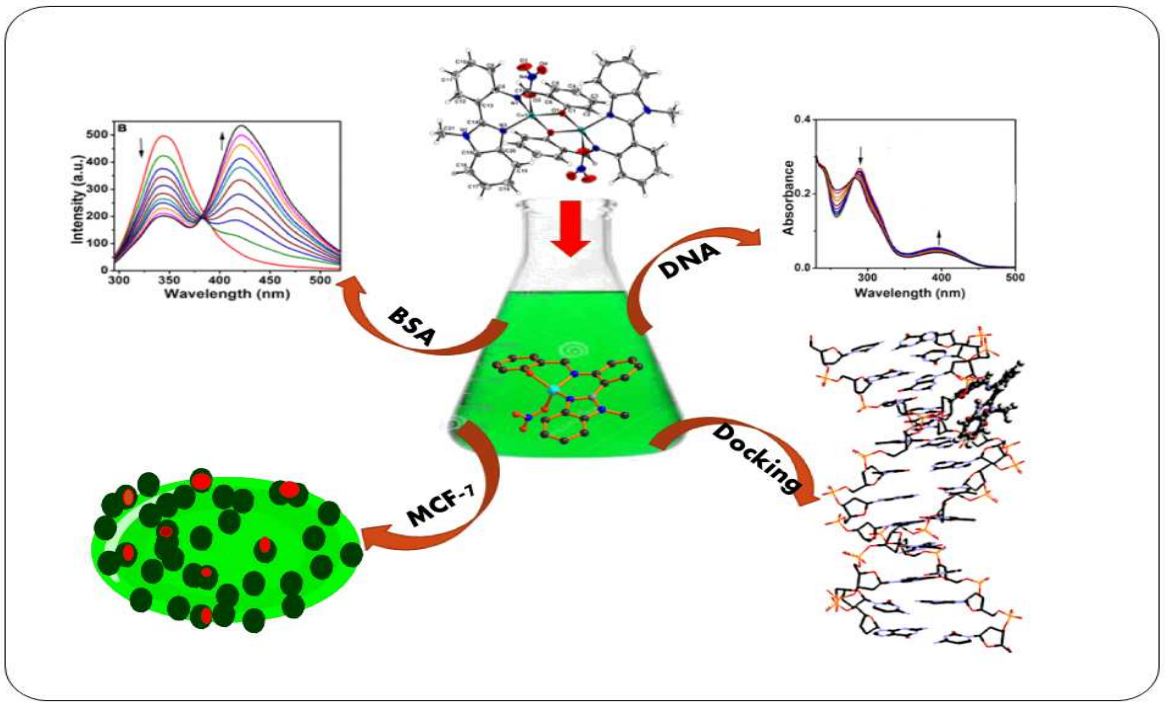

Potential apoptosis inducing agents based on a new benzimidazole Schiff base ligand and its dicopper(II) complex

Anup Paul,[a] Rakesh Kumar Gupta,[a] Mrigendra Dubey,[a] Gunjan Sharma,[b] Biplob Koch,[b] Geeta Hundal,[c] Maninderjeet Singh Hundal,[c] and Daya Shankar Pandey*[a]

[a]Departments of Chemistry and [b]Zoology, Faculty of Science, Banaras Hindu University, Varanasi - 221 005 (U.P.) India

[c]Department of Chemistry, Guru Nanak Dev University, Amritsar - 143005 (Punjab), India

Abstract:

Synthesis, characterization and antiproliferative activity of a new benzimidazole based Schiff base 2-(1-methyl-1-*H*-benzimidazol-2-yl)phenyl)imino)methyl)phenol (**HL**) and dicopper(II) complex [{Cu(**L**)NO_3}$_2$] (**CuL)** containing $\mathbf{L}^-$ has been described. Both **HL** and **CuL** have been meticulously characterized by satisfactory elemental analyses, FT-IR, NMR, ESI-MS, electronic absorption and emission spectroscopy, and their structures unambiguously determined by X-ray single crystal analyses. Titration studies (absorption and emission) revealed interaction of the ligand and its dicopper(II) complex with DNA/BSA and stronger affinity of the **CuL** relative to **HL**. Binding of the **HL** and **CuL** with DNA/BSA have been validated by *in silico* studies and their cytotoxic effect on human breast cancer cell lines (MCF-7) by MTT assay. IC_{50} values (458 μM and 22 μM for **HL**, **CuL**) clearly suggested substantial cytotoxicity of the complex **CuL** toward MCF-7 compared to the ligand **HL**. Greater antiproliferative efficacy of the **CuL** in contrast to **HL** has been evidenced by fluorescence activated cell sorting (FACS) and AO/EB fluorescence staining. Possible mode of apoptotic pathway for **CuL** has further been affirmed by **r**eactive oxygen species (ROS) generation studies.

*** Corresponding author.** E-mail: dspbhu@bhu.ac.in; Tel.: + 91 542 6702480; fax: + 91 542 2368174.

Introduction

Cancer is one of the most fatal non communicable diseases and hundreds and thousands of people die of it every year.[1] To conquer this lethal disease numerous drugs have been discovered and among the metal based drugs, platinum complexes like *cis*-platin, carboplatin, oxaliplatin, etc., have proved to be indispensable in cancer chemotherapy.[2] Although, platinum based drugs find extensive utility in the treatment of cancer, these are associated with numerous dis-advantages.[3] To overcome the limitations associated with '*cis*-platin' and other platinum based anticancer drugs, and to develop those with lower side effects and improved pharmacological properties, attempts are being made to explore non-platinum metal complexes particularly, those capable of binding DNA effectively.[4,5,6] In this context, copper(II) complexes have been promising and present focal theme of the contemporary chemical research.[7] Further, copper ion is capable of directly interacting with DNA/nucleoproteins and tend to cause site-specific damage and, also by binding specific sites it can modify conformational structure of the proteins, polynucleotides, DNA, or membranes.[8] In addition, it has been shown that copper compounds delay cell cycle progression, increase cell death in different cell cultures, and cause apoptosis in cultured mammalian cells which is considered to be crucial for drugs.[9-10]

Furthermore, designing of the metal based drugs have always been associated with synergizing beneficial effect of the ligands and activity of metals to produce a complex with enhanced activity. In this context, selection of organic ligand plays an essential role. As well, antibacterial, antifungal and antimalarial activity of the benzimidazole and its derivatives is well documented.[11-12] The physiological activity and commercial applications of 2-aminobenz-imidazole have received a great deal of attention in recent past, but to our knowledge anticancer activity of the Schiff base metal complexes derived from 2-(2-aminophenyl)-1-*H*-benzimidazole has scarcely been explored.[12] It has been suggested that biological activitiy of Schiff bases are essentially determined by azomethine linkage.[13] With an objective of exploring the role of Schiff base metal complexes as anticancer agents we have chosen 2-(methyl-benzimidazol-2-phenyl)iminomethyl)phenol as a ligand for the present study. Through this contribution we describe synthesis and thorough characterization of benzimidazole based ligand (**HL**) and dicopper(II) complex (**CuL**) derived from it. Also, we present herein binding mode and selectivity of the **HL** and **CuL** toward DNA/BSA, *in silico* studies and their cytotoxicity against human breast cancer cell line (MCF-7).

Results and Discussion

General Properties

The Schiff base ligand 2-(1-methyl-1H-benzoimidazol-2-yl)phenyl)imino)methyl)phenol **(HL)** has been synthesized using 2-(2-aminophenyl)-1H-benzimidazole in two steps. In the first step 2-(2-aminophenyl)-1*H*-benzimidazole has been methylated using sodium hydride and iodomethane in dimethylformamide. In the second step resulting 2-(1-methyl-1H-benzo[d]imidazol-2-yl)-aniline was condensed with salicyldehyde to afford **HL** in reasonably good yield (75%). Synthesis of the complex **CuL** has been achieved by the reaction of a methanolic solution of **HL** with $CuNO_3.3H_2O$ at room temperature under stirring conditions. It has been isolated in ~ 45% yield as olive green crystalline solid. A simple scheme showing synthesis of the **HL** and **CuL** is depicted below in Scheme 1.

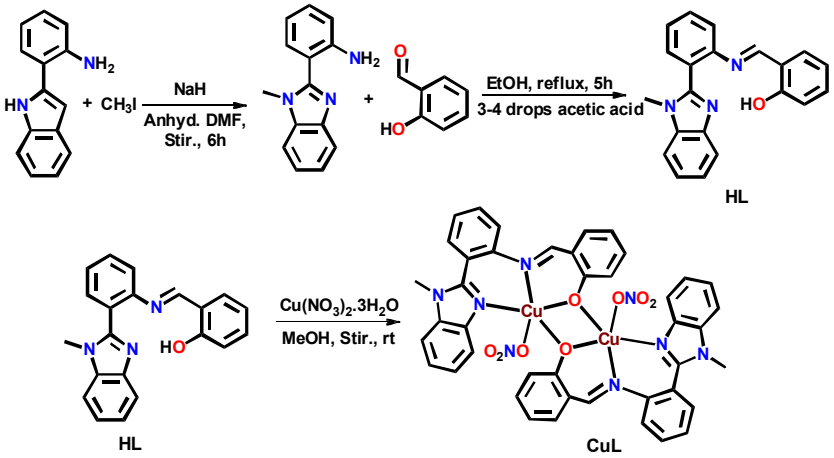

Scheme 1. Showing synthesis of the ligand **HL** and complex **CuL**.

FT-IR spectrum of the free ligand **HL** displays a sharp and strong band at 3287 cm^{-1} attributable to ν_{OH} stretching vibrations. This band disappeared upon coordination of the ligand with metal centre which strongly suggested formation of the **CuL** involving deprotonation of the phenolic group. Further, the band associated with $\nu_{C=N}$ at ~1676 cm^{-1} in the spectrum of the free ligand shifted to lower frequency (~60 cm^{-1}) and clearly indicated coordination of **HL** through imine (C=N) nitrogen. Additionally, appearance of a sharp and strong band at 1384 cm^{-1} along with distinct new bands at 1289, 1030 and 742 cm^{-1} in the spectrum of complex implied presence and coordination of the nitrate anion to metal centre in a monodentate fashion (Fig. S1, ESI†).[20]

^{1}H NMR spectrum of the **HL** dispalyed resonances due to -O*H*, -C*H*=N, and N-CH_3 protons at δ 12.21, 8.60, and 3.68 ppm, respectively. Phenyl ring protons resonated in the range δ 7.82-

6.83 ppm (Fig. S2, ESI†). In the ^{13}C NMR spectrum signals due to phenolic aldimine and methyl carbons appeared at δ 164.30, 160.83 and 30.91 ppm along with other resonances at their usual positions (Fig. S3, ESI†). The positive ion ESI mass spectrum of **HL** displayed molecular ion peak due to $[M + H]^+$ at *m/z* 328.1535 (calcd. 328.1372) along with an additional peak at *m/z* 350.1354 (calcd 350.1269) assignable to $[M + Na]^+$ (Fig. S4, ESI†). On the other hand, **CuL** displayed an essentially important peak due to $[Cu(L)]^+$ at *m/z* 389.1642 (calcd., 389.0589) assignable to mononuclear fragment suggesting dissociation of the dicopper(II) complex into mononuclear species in solution (Fig. S5, ESI†).

Dissociation of the **CuL** into mononuclear species has further been authenticated by ESR studies. X-band EPR spectrum of the **CuL** has been acquired both in the solid state as well solution (DMSO) at liquid nitrogen temperature (LNT). At 77K the solid polycrystalline **CuL** showed a single broad-band ESR spectrum with g value of 2.10 (Fig. S6, ESI†) which suggested magnetic interaction between the copper centres through phenoxy oxygen bridges. On the other hand, solution (DMSO) EPR spectrum of **CuL** at 77K dispalyed predominant EPR-active species which is quite different from that in the solid state (Fig. S6, ESI†). It exhibited a major signal with S = 1/2 and observed $g_{\perp}$, $g_{\parallel}$, $A_{\parallel}$ values of 2.073, 2.417 and 2.199, 155 X 10^{-4} cm^{-1}, respectively, typical for a mononuclear species.[15,16] From the EPR studies we conclude dissociation of the dicopper complex into mononuclear species in solution, which is in accord with the observations made from ESI-MS studies.

The electronic absorption spectra of **HL** (DMSO:H_2O, v/v, 1:99) displayed one intense absorption band at 282 nm assignable to the $n \rightarrow \pi^*$ transition associated with azomethine group (-C(H)=N). Upon complexation with the copper(II) centre absorption band experienced a red shift of ~7 nm and occurred at 289 nm with an increase in the absorption intensity. It strongly suggested the coordination of **HL** with copper(II) through azomethine nitrogen (-C(H)=N).[17] In addition, **CuL** dsipalyed a strong band at 396 nm attributable to ligand-to-metal charge transfer transition (phenoxy-to-copper) (Fig. S7, ESI†).[18]

The crystal structure of **HL** revealed the rotation of phenolic and benzimidazole rings with respect to central phenyl rings by a dihedral angle of 28.45(8) and 68.37(6)°, respectively between them. In the process benzimidazole ring becomes almost perpendicular to the phenol ring (dihedral angle 85.77(6)° (Table S1). This conformation brings the O-H group under influence of imidazole ring leading to O-H…π interactions (O…centroid 3.805(6), H…centroid

3.275(7) Å) (Table S2). Strong intramolecular H-bonding interactions have been observed between the OH group (O1) and imine nitrogen (N1), water molecule O1W and imidazole nitrogen N3 (Fig. S8, ESI†). The water molecules in the crystal structure have a very interesting supramolecular arrangement whereby both O1W and O2W form three H-bonds to each other. This arrangement forms 1D undulating infinite tapes of water molecules running parallel to the 'a'- axis (Fig. 1b) and may be assigned as T4(2) according to the nomenclature used for water clusters in organic molecular crystals.[19]

T4(2) kind of arrangement of the water molecules is rather rare. It has been known as a part of other Tn(q)m(r) infinite tapes in a few cases e.g. as T4(2)6(2) (found in 24 cases), T4(2)10(2) (found in 5 cases) but then[19] there is only one known structure having the T4(2) motif as such, out of 1430 structures considered as having various water assemblies in organic molecules only. The tape in that case has been formed by two lattice water related by a twofold axis of rotation, here these are related by a centre of inversion. A fresh search on CSD shows ten hits with such a motif.[20] The organic molecule **HL** is tethered to these tapes by O1W…N3 (benzimidazole) H-bonding interactions (Fig. 1b).

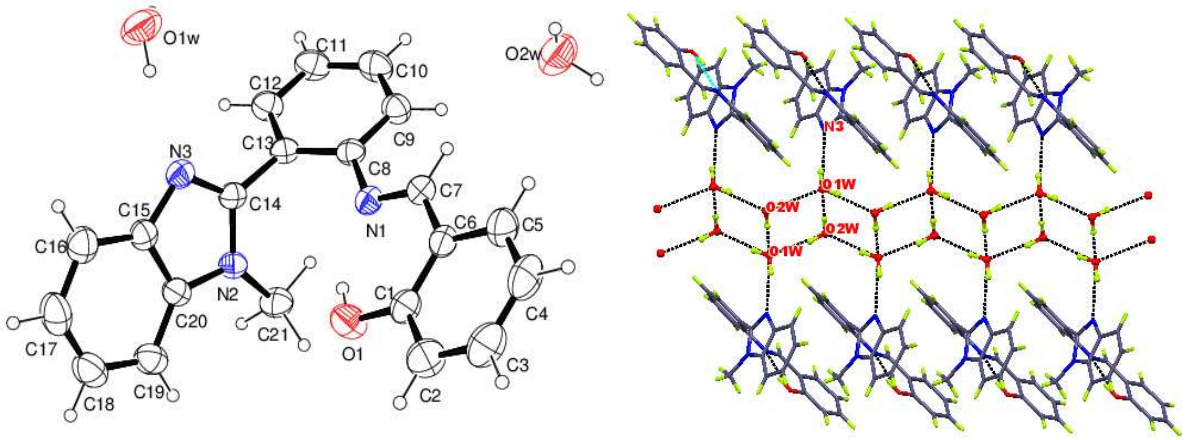

(a) (b)

Fig. 1 ORTEP diagram of the ligand **HL** along with the two lattice water molecules at 30% probability (a) Showing the self-assembly of water molecules to form corrugated T4(2) tapes. The ligand molecules are tethered to this ribbon by water…imidazole (O1W…N3) H-bonding interactions (b).

The complex **CuL** presents a centrosymmetric dimer with phenolic groups bridging two copper(II) centres (Fig. 2). In comparison to free ligand **HL** the phenol ring and benzimidazole on complexation with metal centre exhibited higher and lower rotations, respectively with

regard to the central phenyl ring (dihedral angles 54.07(11)° and 43.70(9)°, respectively). The coordination environment about each copper(II) centre may be regarded as distorted square pyramidal with the Addison parameter[19] $\tau = 0.51$ ($\tau = (\beta-\alpha)/60$, where α and β are the larger basal angles with $\beta > \alpha$) and its value may vary from 0, representing ideal sp to 1, denoting ideal tbp geometry). The bridging phenolic oxygen, O1 and $O1^{i}$, benzimidazoline nitrogen N3 and imine nitrogen N1 lie in the basal plane and nitrate oxygen O2 occupies the axial position. Cu1-O1 and Cu1-$O1^{i}$ bond distances are 1.966 (2) and 1.975 (2) Å, respectively thereby giving rise to Cu_2O_2 core (where I = -x+2, -y+2, -z) (Table S1).

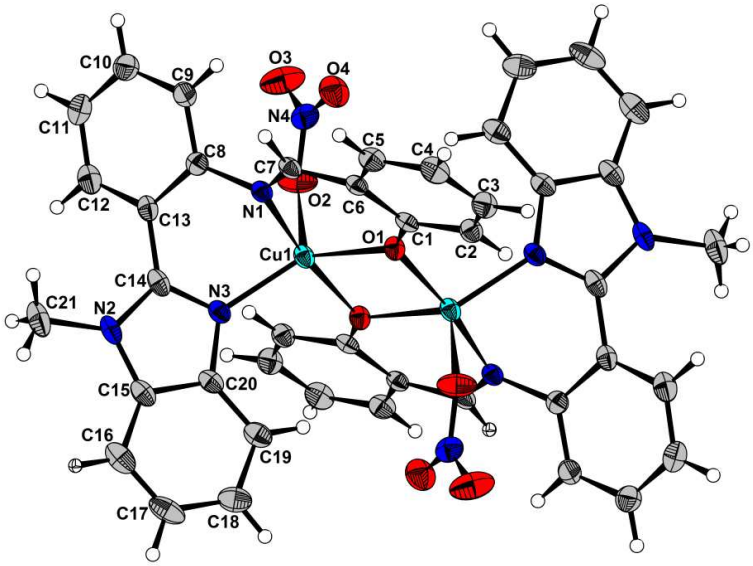

Fig. 2 ORTEP diagram of the **CuL** complex at 50% probability.

The Cu1···$Cu1^{1}$ separation within the dimer is 3.071 (1) Å which is comparable with those reported previously.[21,22] Remaining two oxygens of the nitrate groups are involved in weak intermolecular H-bonding with the aryl carbons of the adjacent molecules and form 1D chain running parallel to 'a'- axis (Fig. S9, ESI†).

DNA interaction studies

Electronic absorption titration

The binding mode and extent of binding of the metal complexes with DNA can be successfully followed by electronic absorption spectroscopy.[23,24] Binding behaviour of **HL** and **CuL** (H_2O:DMSO, 95:5) with CT DNA has been studied by absorption titration studies. UV-vis absorption spectra of both **HL** and **CuL** in absence and presence of CT DNA is shown in Fig. 3.

Upon gradual addition of CT DNA (0-30 μL) to their respective solutions the ligand centered intra-ligand band (~280 nm) for these compounds displayed hypochromism (23%, **HL**; 10%, **CuL**). Notably, **HL** did not show any significant shift in the position of band while **CuL** exhibited a blue shift of ~7 nm (289 to 282 nm). At the same time, for **CuL** the band at 396 nm exhibited hyperchromism (27%) without any appreciable shift. It suggested electrostatic interaction of **HL/CuL** with DNA *via* electrostatic and intercalation mode. To compare DNA binding affinity of these compounds intrinsic binding constants (K_b) have been evaluated using following equation 1:[25]

$$[DNA]/(\varepsilon_a - \varepsilon_b) = [DNA]/(\varepsilon_b - \varepsilon_f) + [DNA]/(\varepsilon_a - \varepsilon_f) \quad \text{..... (1)}$$

where [DNA] is the concentration of DNA, ε_a is apparent extinction coefficient obtained from A_{obs}/[complex] and ε_f and ε_b are the extinction coefficients for compounds in its free and bound state, respectively.

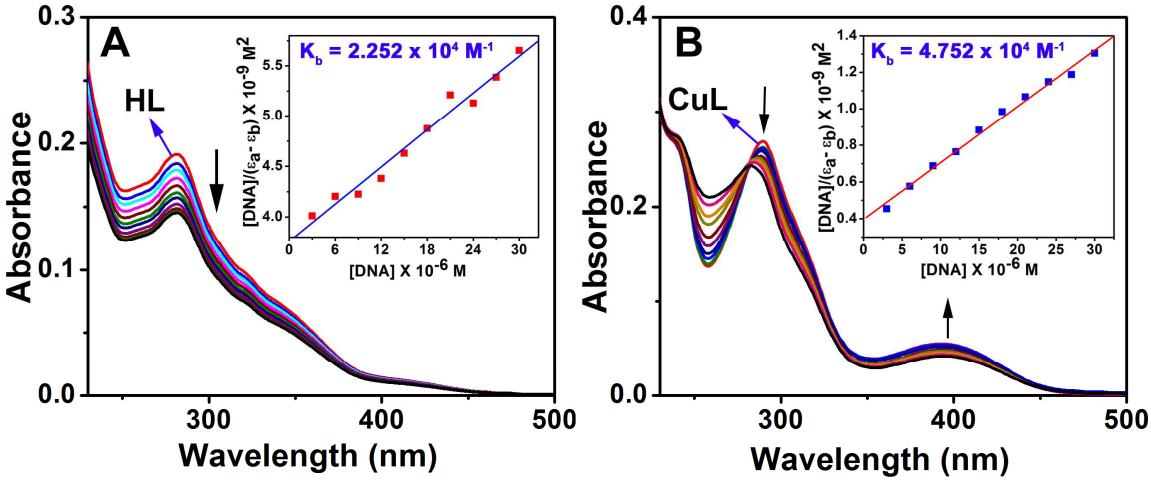

Fig. 3 Absorption titration spectra of **HL** (A) and **CuL** (B) with an increase in the concentration of CT DNA to complex (0–30 μM) at rt. Arrow shows the absorbance changes upon increasing CT DNA concentration. Inset shows the plots of $[DNA]/(\varepsilon_a-\varepsilon_f)$ *vs*. [DNA].

The binding constant 'K_b' has been calculated from the ratio of the slope to intercept of the plot $[DNA]/(\varepsilon_a - \varepsilon_b)$ *vs* [DNA] (inset, Fig. 3). Calculated values of K_b for **HL** and **CuL** came out to be 2.252×10^4 M^{-1} and 4.752×10^4 M^{-1}, respectively and revealed that **CuL** shows better binding affinity than **HL**. The observed K_b values are comparable to those for other copper(II)

complexes and we conclude that both the compounds display good binding affinity toward DNA through electrostatic interactions.

EB-DNA Experiment

Competitive binding studies using ethidium bromide (EB) bound to DNA (EB–DNA) has been used to elucidate the binding affinity of **HL** and **CuL**. Binding of these compounds exhibited a decrease in the emission intensity of EB–DNA suggesting displacement of the EB which is characteristic feature of the intercalators.[26] The emission spectra of EB and EB–DNA in absence and presence of **HL** and **CuL** (0–30 μM) is depicted in Fig. 4. It clearly shows that addition of the compounds under study to EB–DNA (λ_{em} = 603 nm) complex leads to quenching of the emission intensity by 51 and 75%, respectively. The present study illustrated that both **HL** and **CuL** efficiently compete with EB for the intercalative binding sites of DNA by replacing EB, particularly for **CuL**.[27] Further, quenching strength of **HL** and **CuL** toward EB–DNA complex have been calculated using Stern-Volmer equation shown below (equation 2):

$$F_0/F = Kq\,[Q] + 1 \quad \text{..... (2)}$$

where, F_0 is the emission intensity in absence of the compounds, F is the emission intensity in presence of the quencher, Kq is the quenching constant and Q is concentration of compounds. The Kq values have been obtained from the slope of the F_0/F vs. [Q] plot. The S-V plots for **HL** and **CuL** are shown in the inset of Figs. 4 (A) and (B) respectively.

The quenching constant K_q for **HL** and **CuL** (4.004×10^4 M^{-1} and 9.853×10^4 M^{-1}) has been deduced following equation 2 and using F_0/F vs [Q] plot. The higher K_q value for **CuL** indicated its greater ability to replace EB relative to **HL**, which is consistent with the conclusions drawn from absorption titration studies. Further, apparent binding constants (K_{app}) have been calculated using equation 3:

$$K_{EB}[\text{EtBr}] = K_{app}[\text{complex}] \quad \text{.....(3)}$$

where, [complex] is the value at 50% decrease of the fluorescence intensity for EB, K_{EB} (1.0×10^7 M^{-1}) is DNA binding constant for EB, [EB] is concentration of EB = 10 μM. The K_{app} values came out to be 2.72×10^4 M^{-1} (**HL**) and 5.36×10^5 M^{-1} (**CuL**). These follow the order **CuL** > **HL** which is in good agreement with the observations made from absorption spectral studies.

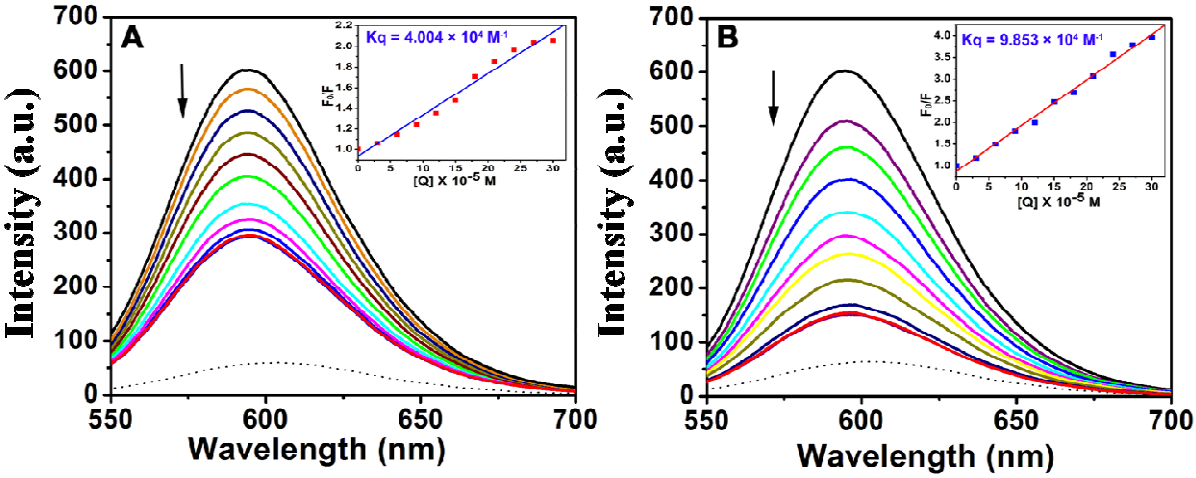

Fig. 4 Emission spectrum of EB bound to DNA in absence (---) and presence of **HL** (A) and **CuL** (B). [EB] = 10 μM, [DNA] = 10 μM, [**HL**/**CuL**] = 0–30 μM. Arrow shows changes in emission intensity upon incremental addition of **HL** and **CuL**. Inset shows the Stern-Volmer plots of F_0/F *vs*. [Q].

BSA binding studies

Binding affinity of the **HL** and **CuL** with BSA has been followed by tryptophan emission quenching using BSA solution. Emission of the BSA arises due to presence of tryptophan, tyrosine, and phenylalanine residues. Its emission intensity depends on the extent of exposure of the tryptophan residues, nearby polar environment and the quenching groups through molecular interactions. Protein binding affinity has been studied by addition of increasing amounts of **HL** and **CuL** (0–30 μM) to BSA (0.5 μM) at rt by following decrease in the fluorescence intensities (λ_{exi} = 280 nm; λ_{emi} = 345 nm).[28] The fluorescence spectra of BSA in absence and presence of the **HL** and **CuL** is depicted in Fig. 5. It is observed that fluorescence intensity of BSA quenched by 18% without any significant shift upon gradual addition of **HL**. On the other hand addition of **CuL** led to a substantial decrease in the intensity (74%) with a small blue shift (1-2 nm) which suggested that fluorophore of the BSA is placed in hydrophobic environment.

The fluorescence spectral changes indicated that both **HL** and **CuL** bind with protein.[28] It is noteworthy to mention that in addition to fluorescence quenching for BSA at 343 nm, a continuous increase in the luminescence band at 429 nm has been observed in the presence of **HL** and **CuL**. This quenching of BSA fluorescence and appearance of luminescence may be due

to energy transfer from the excited state BSA to ligand and the metal complex (FRET) and also, due to the strong overlap of the fluorescence spectrum of the tryptophan (Trp) of BSA and absorption spectrum of the compounds.[29]

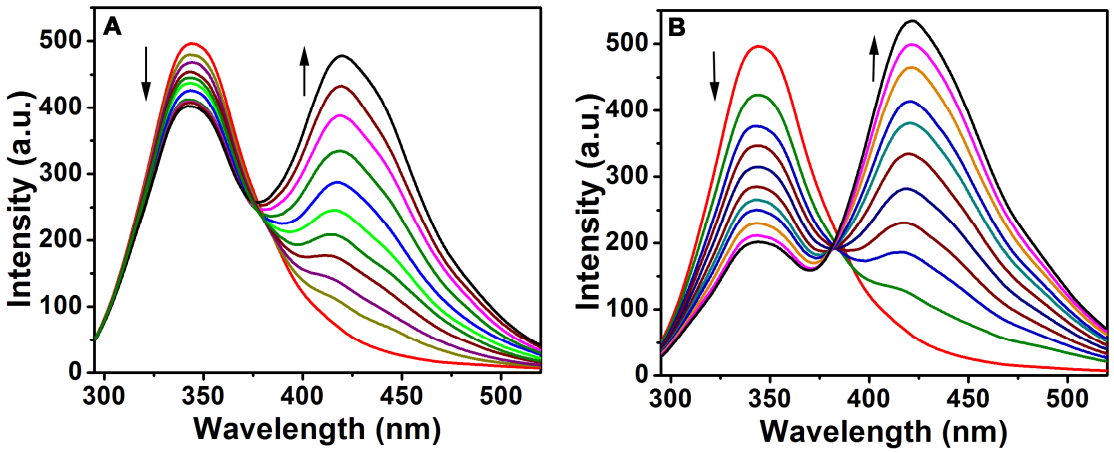

Fig. 5 Emission spectrum of BSA (1×10^{-6} M; $\lambda_{exi,}$ 280 nm; $\lambda_{emi,}$ 345) in presence of increasing amounts of **HL** (A) and **CuL** (B) (0–30 μM). Arrow shows emission intensity changes with increasing concentration.

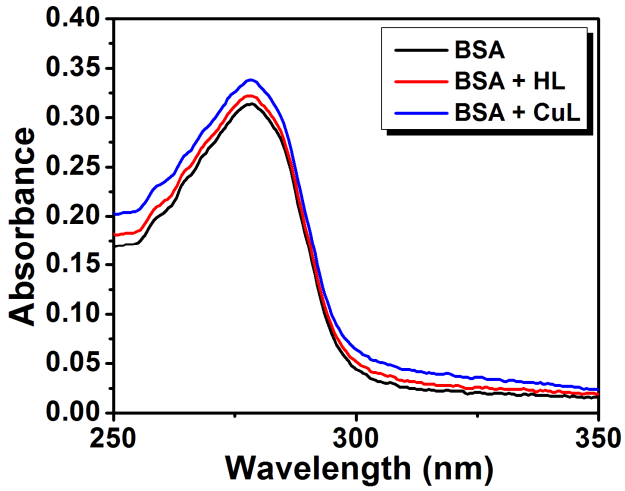

Fig. 6 UV-vis absorption spectra of BSA (10 μM) in the presence of **HL** and **CuL**.

To verify quenching mechanism, UV-vis absorption spectra of BSA in presence of HL and CuL have been acquired. In dynamic quenching mechanism the UV-vis spectrum of BSA do not show any change whereas in static quenching BSA exhibits alterations in the UV-vis spectrum due to formation of a complex with the drug. From Fig. 6 it is clear that the absorbance of BSA

before and after addition of HL/CuL exhibited significant change at ~ 280 nm. The changes observed in this study directly demonstrate ground state complex formation between BSA and HL/CuL, thus it is concluded that fluorescence quenching of BSA takes place by static quenching.

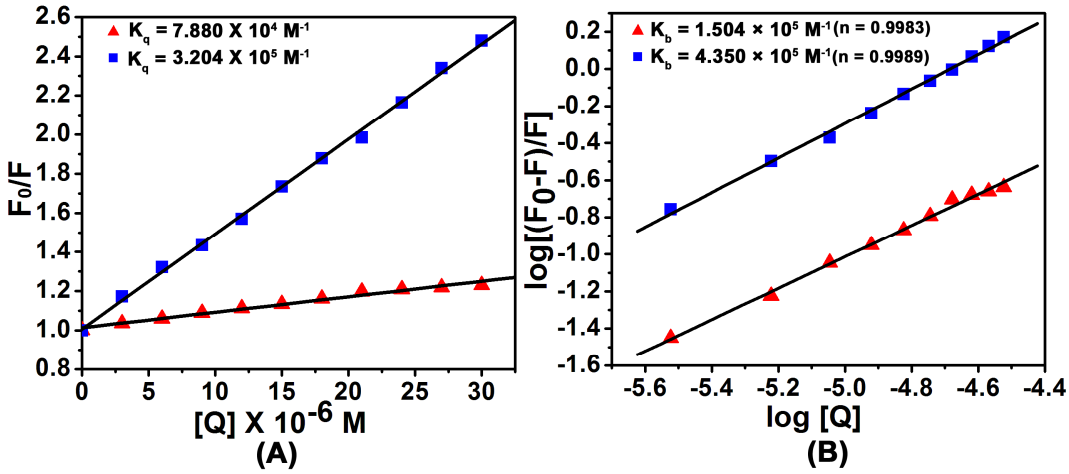

Fig. 7 ST-Volmer (A) and Scathered (B) plots of the BSA fluorescence titration data of the **HL** (red) and **CuL** (blue).

To measure the extent of quenching, K_q have been calculated using Stern-Volmer equation [Eqn. 1, Fig. 7 (A)]. Values of the K_q obtained from the slope of F_0/F *vs.*[Q] has been found to be 7.880 × 10^4 M^{-1} and 4.350 × 10^5 M^{-1} for **HL** and **CuL**, respectively. Further, number of binding sites (n) and binding constant (K_{bin}) have been evaluated by Scatchard equation:

$$\log [(I_0 - I)/I] = \log K_b + n \log [Q] \quad \text{.....(4)}$$

Where, K_b is the binding constant of the compound with BSA and n is the number of binding sites. The K_b (3.220 × 10^5, **HL**; 4.350 × 10^5 M^{-1}, **CuL**) has been determined from the slope of the plot of log $[(F_0 - F)/F]$ *vs*. log $[Q]$ [Fig. 7 (B)]. The evaluated n values for both the compounds fall close to ~1 and indicate the existence of a single binding site. Results from the above studies clearly indicated high binding affinity of **CuL** relative to **HL** which is in agreement with the trends observed from DNA binding affinities.

Synchronous fluorescence spectroscopic studies

Synchronous fluorescence spectroscopy has been used to gather information about the environment in close vicinity of the fluorophores, such as tryptophan and tyrosine residue.[34] In

this context synchronous fluorescence spactra has been acquired with concurrent scanning of the excitation and emission monochromators by keeping a constant wavelength difference (Δλ) 15 and 60 nm.[30] The effect of **HL** and **CuL** (0–30 μM) on synchronous fluorescence spectra of the BSA was acquired both at Δλ 15 and 60 nm (Figs. S11–S12, ESI†). The spectrum of BSA at Δλ 15 nm in presence of the compounds exhibited a decrease in the fluorescence intensity at 288 nm (20%, **HL;** 43%, **CuL**) without any appreciable shift in the position of the band (Figs. S11, ESI†). On the other hand the spectrum at Δλ 60 nm also displayed quenching of the fluorescence intensity at 280 nm (28%, **HL**; and 65% **CuL**) without any significant shift (Figs. S12, ESI†). It clearly indicated that fluorescence intensity of both tryptophan and tyrosine diminished with increasing concentration of **HL** and **CuL**. Thus, synchronous fluorescence measurements substantiated that both **HL** and **CuL** effectively bind with BSA and affects the conformation of both tyrosine and tryptophan micro-regions.[30]

Docking studies

To have better understanding of interaction mode of the complex with DNA and HSA mononuclear species have been optimized using molecular mechanics universal force field simulation (MMUFF)[31] prior to docking studies considering dissociation of the dicopper(II) complex into mononuclear species in solution as evidenced by ESI-MS and EPR studies.

Molecular docking with B-DNA

Molecular docking studies on **HL** and **CuL** has been carried out with B-DNA (PDB ID: 1BNA). In this study **HL** and **CuL** have been successively docked with DNA to predict the appropriate binding site and preferred orientation inside DNA minor groove. Energetically most favorable conformation for the docked structures for **HL** and **CuL** are depicted in Fig. 8 (A) and Fig. 8 (B), respectively. It revealed binding of both **HL** and **CuL** with the minor groove of targeted DNA due to their enantioselectivity and site-specificity toward A-T rich region. Further, resulting structures are stabilized by van der Waals interaction and hydrophobic contacts with DNA.[32] Relative binding energies of the docked model of **HL** and **CuL** with DNA have been found to be –233.8 kJ mol^{-1} and –285.36 kJ mol^{-1}, respectively. These are consistent with the results obtained from spectral studies and indicated greater binding affinity of CuL relative to HL.

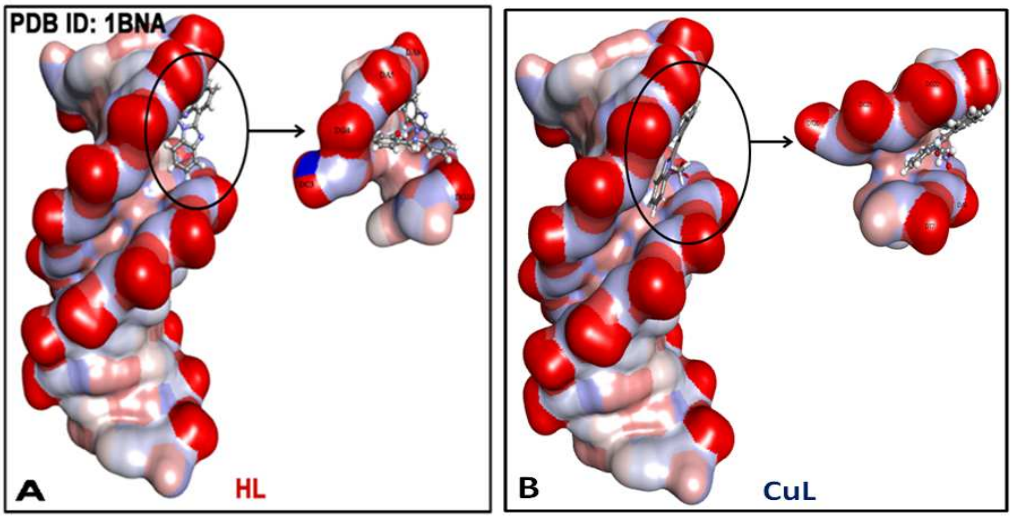

Fig. 8 Docked structures in presence of **HL** (A) and **CuL** (B) with DNA.

Similarly, molecular docking studies have been performed to further rationalize potential binding sites and interactions of the **HL** and **CuL** with HSA. The choice of HSA for docking studies is based on its structural homology with BSA and this study may provide deep information about the human protein binding interactions. The 3D structure of HSA has been taken from the protein data bank (PDB.ID: 1HA2). It contains three homologous domains: doamin I (residues 1-195), II (196-383) and III (384-585). Each domain consists of two subdomains (A and B) and these are further divided into nine loops by 17 disulfide bonds each one formed by six helices and its secondary structure is dominated by α-helix.[33] The major binding sites of HSA are usually hydrophobic cavities in the subdomains IIA and IIIA as well as tryptophan (Trp-214) and tyrosine residues present in subdomain IIA and in site II, respectively.[34] Molecular docking studies on **HL** with HSA revealed that protein-ligand interaction takes place at site I (subdomain IIA) in proximity to the hydrophobic residues such as LEU 115, VAL 116, ARG 117, MET 123, ILE 142, TYR 161, LEU 182, ARG 186 and LYS 190 (within 4 Å) and implied the existence of hydrophobic interaction between them (Fig. S13, ESI†).

On the other hand, docking studies on **CuL** with HSA showed that it resides in close vicinity to the hydrophobic residues of site I at subdomain IIIA like ARG114, LEU115, VAL116, ARG117, ILE142, HIS146, TYR161, ARG186, GLY189, LYS190, SER193, ARG197 (within 4 Å) (Fig. 9).

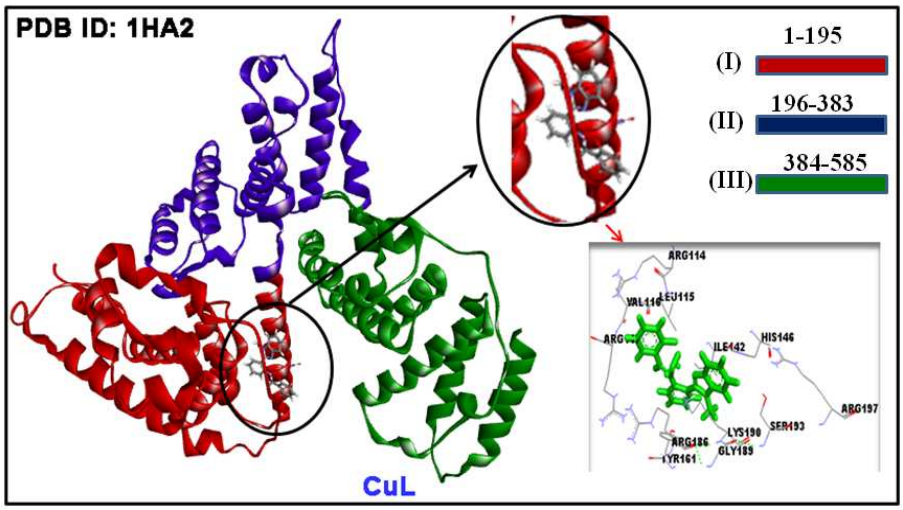

Fig. 9 Structure showing location of **CuL** within the hydrophobic pocket of HSA (PDB ID: 1HA2).

Thus the results from molecular docking studies revealed that interaction between **HL** and **CuL** with HSA is dominated by hydrophobic forces. These results also provide a good structural evidence to explain efficient fluorescence quenching of the BSA fluorophore in presence of these compounds.

***In vitro* cytotoxicity assay**

Cytotoxicity of the **HL** and **CuL** has been tested *in vitro* against human breast adeno-carcinoma cell line (MCF-7) by MTT assay. MTT assay analysis revealed that both **HL** and **CuL** exhibit significant inhibitory effects on proliferation of MCF-7 cells in the range 458-610 μM and ~22 μM, respectively**.** The results from MTT assay suggested that **CuL** is more effective relative to **HL** itself and can induce cytotoxicity at very low concentrations (Fig. S14, ESI†).

Cell cycle analysis by flow cytometry

Flow cytometry is one of the most powerful and specific methods for integrated study of the molecular and morphological events occurring during the cell death. Cell cycle is an important phenomenon that plays a crucial role in the developmental pathways and is frequently deregulated in many cancerous diseases.[36,37] Thus, to investigate the cell death and cell cycle delay on the basis of DNA content in MCF-7 cells fluorescence activated cell sorting (FACS) has been undertaken with PI staining (Fig. 10).

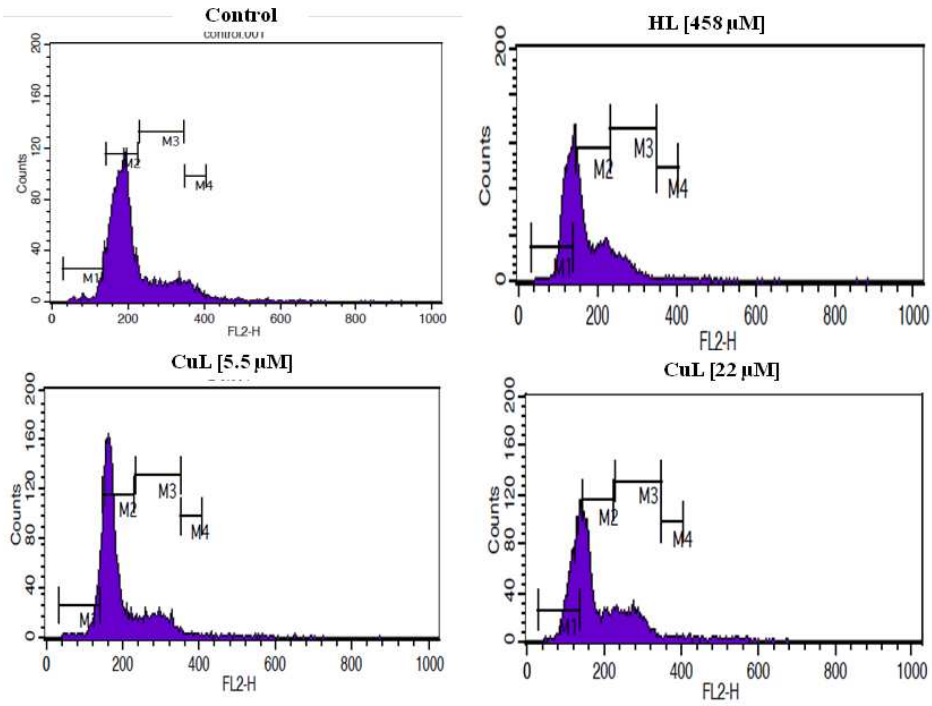

Fig. 10 DNA fluorescence flow cytometric profiles of PI-stained MCF-7 cells after 24h incubation for control and treated with different concentrations of **HL** and **CuL**.

The experiments have been performed on the basis of IC50 value of the HL (458 μM) and CuL (22 μM) as shown in Fig. 10. FACS analysis showed that percentage of the sub-G1 cells enhanced significantly upon treatment with **CuL** as compared to that for control. The cell cycle distribution of the control MCF-7 cells were 4.1% in sub-G1, 68.8% in G1, 16.99% in S and 4.8% in G2/M, when the cells were treated with complex **CuL** the cell cycle distribution arose to: sub-G1 29%, G1 40.43%, S 20.38% G2/M 0.74% whereas when the cell were treated with **HL** it turned out to be: Sub-G1 35.76%, G1 39.75%, S 13.37 G2/M 0.55% (Fig. 10) . These data clearly indicated that **CuL** can induce cell cycle delay in S phase of the cell cycle. At near to IC50 value a dramatic decrease of the cells in G2/M phase has been detected. However, for both **HL** and **CuL** lightly fluctuating trend in the percentage of cells in S phase has been observed. In particular, both HL and **CuL** influences the growth and proliferation of MCF-7 cells close to their IC50 value. But higher percentage has been observed in S phase in **CuL** treated cells as compared to control and **HL** treated cells.

Apoptosis analysis by fluorescence microscope

To quantify the early and late apoptotic cells these have further been scored under fluorescence microscope. Acridine orange (AO) stained both apoptotic and viable cells emit green fluorescence when bound to double stranded DNA and red fluorescence to single stranded RNA. For the said experiment different concentrations of compounds (305, 458 and 610 μM of HL and 11, 22 and 33 μM of CuL) have been chosen along with their IC_{50} value for morphological analysis of apoptosis on MCF-7 cells. Fluorescence microscopic analysis revealed that both **HL** and **CuL** are able to induce apoptosis in MCF-7 cell line. The apoptotic cells increases with increasing concentration of the **HL** and **CuL**, respectively. However, with **CuL** more apoptotic cells were observed than **HL** with their increasing concentrations, control cells did not show any cell death. When the cells were treated with concentrations higher than their IC_{50} value for **CuL**, most of the treated cells underwent necrosis as compared to **HL** treated cells (Fig. 11).

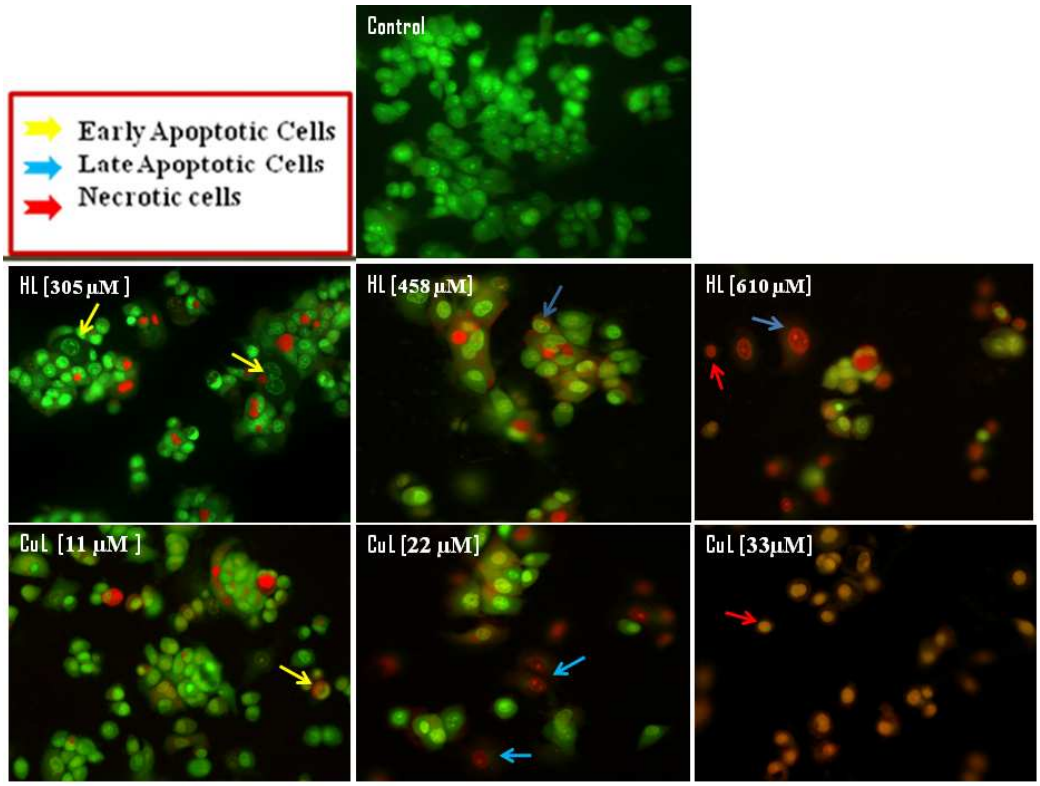

Fig. 11 Images of the drug treated MCF-7 cells after treatments with different concentrations of **HL** and **CuL** for 24 h and staining with AO/EB.

CuL induced ROS production in MCF-7 cells

Apoptosis may occur in the cells by several mechanisms and most of the copper complexes induce this process by increasing the level of intracellular reactive oxygen species (ROS).37 To explore the probable mechanism for cell death by CuL in the present study intracellular ROS generation has been follwed using DCFH-DA dye in the treated as well as in control cells. In this regard, MCF-7 cells were treated with CuL (0, 22 and 33 μM) for 24 h for ROS detection. It was observed that after treatment with the copper complex ROS generation enhanced and showed an increase in a dose dependent manner. (Fig. 12).38 Here we simply conclude that the apoptosis in the presence of CuL takes place due to enhanced ROS level.

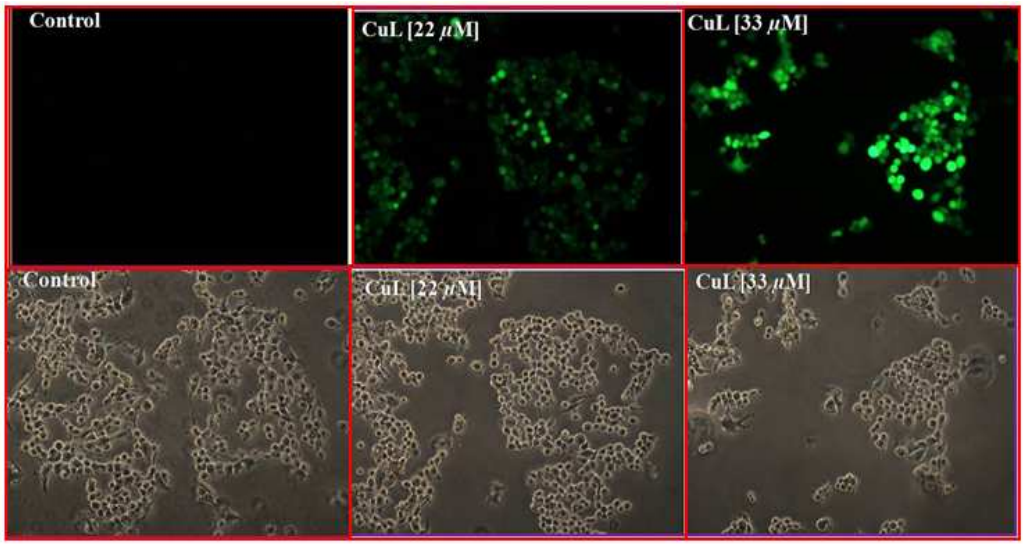

Fig. 12 Generation of ROS induced by CuL in MCF-7 cells

Conclusions

In conclusion, a new benzimidazole based ligand **HL** and its dicopper(II) complex **CuL** have been designed synthesized and well characterized. It has been established that both **HL** and **CuL** effectively bind to DNA through partial intercalative/electrostatic interactions. These also found to interact with protein (BSA) which has been supported by UV/visible, fluorescence and synchronous spectroscopy. Further, molecular docking studies suggested that both ligand and complex bind with minor groove of the DNA through electrostatic interaction, whereas in protein, ligand binds with the hydrophobic residues of site I at subdomain IIA and complex binds with the hydrophobic residues of site II at subdomain IIIA. The dicopper(II) complex **CuL** has been found to be more active drug than the ligand as reflected from their K_b values and IC_{50} [458

(**HL**) and 22 μM (**CuL**)] values towards MCF-7 cancer cell line. The induction of apoptosis by **HL** and **CuL** has further been established by AO/EB staining and FACS with PI staining and ROS. This study provides deep insight and understanding toward the mechanism of interactions of newly synthesized **HL** and **CuL** with serum albumin and DNA, necessary for the development of potential anticancer agents. Besides, increasing ROS generation suggested that **CuL** may be a potent antitumor agent toward MCF-7 cells by inducing apoptosis *via* a ROS-triggered apoptotic pathway. Further, the results from the present study suggest that these compounds merits further investigation as a new drug and modifications of the ligand may improve anticancer activity and dissolution properties of the resulting new drugs.

Acknowledgements

We thank to the DST, New Delhi, India for financial assistance through the scheme SR/S1/IC-25/2011. A. P acknowledges the financial support from University Grants Commission, New Delhi, India through DSK-PDF fellowship (grant F. No. 4-2/2006 (BSR)/13-788/2012 (BSR). We are also thankful to the Head, Departments of Chemistry and Zoology, Faculty of Science, Banaras Hindu University, Varanasi (U.P.) India, for extending laboratory facilities. We also kindly acknowledge the Centre for Bioinformatics, Banaras Hindu University, Varanasi (U.P.) India for carrying out *in silico* studies.

Supporting Information

Electronic Supplementary Information (ESI) available: CCDC deposition Nos. CCDC 1005120-1005121, experimental procedures, synthesis and characterization, Figs. S1–S14 containing IR, ^{1}H and ^{13}C NMR, ESI-MS, UV/vis, fluorescence, docking materials and Table S1–S2.

References

1 American Cancer Society, Global Cancer -Facts & Fig.s 2007, p. 1. ENCYCLOPEDIA OF SCIENCES /&2001 Nature Publishing Group

2 (a) Lloyd Kelland, *Nature Reviews Cancer,* 2007, **7**, 573-584. (b) X. Wang and Z. Guo, *Chem. Soc. Rev.*, 2013, **42**, 202.

3 P. C. A. Bruijnincx and P. J. Sadler, *Curr. Opin. Chem. Biol*., 2008, **12**, 197

4 (a) G. Suss-Fink, *Dalton Trans.*, 2010, **39**, 1673. (b) C. M. Che and R. W. Y. Sun, *Chem. Commun.*, 2011, **47**, 9554. (c) N. P. E. Barry and P. J. Sadler, *Chem. Commun.*, 2013, **49**, 5106. (d) R. Trondl, P. Heffeter, C. R. Kowol, M. A. Jakupec, W. Berger and B. K. Keppler, *Chem. Sci.*, 2014, *DOI: 10.1039/C3SC53243G.*

5 A. R. Kapdi and J. S. Fairlamb, *Chem. Soc. Rev.*, 2014, **43**, 4751.

6 (a) S. K. Hadjikakou and N. Hadjiliadis, *Coord. Chem. Rev*., 2009, **253**, 235. (b) T. S. B. Baul, A. Paul, L. Pellerito, M. Scopellitib, C. Pellerito, P. Singh, P. Verma, A. Duthied, D deVos, R. P. Verma and U. Englert, *J. Inorg. Biochem*., 2010, **104**, 950. (c) T. S. B. Baul, A. Paul, L. Pellerito, M. Scopellitib, C. Pellerito, P. Singh, P. Verma, A. Duthied, D de Vos, R. P. Verma, and U. Englert, *J. Inorg. Biochem*., 2012, **107**, 119.

7 (a) S. Lim, B. M. Paterson, M. T. F. Tavoletti, G. J. O'Keefe, R. Cappai, K. J. Barnham, V. L. Villemagne and P. S. Donnelly, *Chem. Commun*., 2010, **46**, 5437. (b) D. S. Raja, G. Paramaguru, N. S. P. Bhuvanesh, J. H. Reibenspies, R. Renganathan and K. Natarajan, *Dalton Trans*., 2011, **40**, 4548. (c) D. S. Raja, N. S. P. Bhuvanesh and K. Natarajan, *E. J. Med. Chem*., 2011, **46**, 4584. **(d)** R. Loganathan, S. Ramakrishnan, E. Suresh, A. Riyasdeen, M. Akbarsha and M. Palaniandavar, *Inorg. Chem.*, 2012, **51**, 5512. (e) M. G. Álvarez, A. P. Álvarez, L. del C. Agudo, A. Castiñeiras, M. L. González, J. Borrás and G. A. Piña, *Dalton Trans*., 2013, **42**, 10244. (f) M. J. Li,T. Yu Lan, X. H. Cao, H. H. Yang, Y. Shi, C. Yi and G. N. Chen, *Dalton Trans.*, 2014, **43**, 2789. (g) C. Santini, M. Pellei, V. Gandin, M. Porchia, F. Tisato and C. Marzano**,** *Chem. Rev.*, 2014, ***114***, 815.

8 (a) C. Marzano, M. Pellei, D. Colavito, S. Alidori, G. G. Lobbia, V. Gandin, F. Tisato and C. Santini, *J. Med. Chem*., 2006, **49**, 7317. (b) C. Marzano, M. Pellei, F. Tiasto and C. Santini, *Anticancer Agents Med. Chem.,* 2009, **9**, 185. (c) A. T. Chaviara, P. C. Christidis, A. Papageorgiou, E. Chrysogelou, D. J. Hadjipavlou-Litina and C. A. Bolos, *Inog. Biochem*., 2005, **99**, 2102.

9 E. R. Jamieson and S. J. Lippard, *Chem. Rev*., 1999, **99**, 2467.

10 S. Tardito, O. Bussolati, M. Maffini, M. tegoni, M. Giannetto, V. Dall'Asta, R. Franchi-Gazzola, M. Lanfranchi, M. A. Pellinghelli, C. Mucchino, G. Mori and L. Marchio, *J. med. Chem.*, 2007, **50**, 1916.

11 (a) K. F. Ansari and C. Lal, *Eur. J. Med. Chem.,* 2009, **44**, 4028. (b) J. Camacho, A. Barazarte, N. Gamboa, J. Rodrigues, R. Rojas, A. Vaisberg, R. Gilman, J. Charris, *Biorg. Med. Chem.,* 2011, **19**, 2033.

12 (a) M. Alp, H. Goker, R. Brun and S. Yildiz, *Eur. J. Med. Chem.,* 2009, **44**, 2002. (b) M. Sunitha, P. Jogi, B. Ushaaiah, C. Gyanakumari, *Journal of Chemical and Pharmaceutical Research*, 2012, **4**, 1553. (c) Y. Garg, M. K. Samota, G. Seth, *Asian Journal of Chemistry* 2005, 17, 615.

13 B. S. Holla, B. Veerendra, M. K. Shivananda, B. Poojary, *Eur. J. Med. Chem.,* 2003, **38**, 759. (b) B. S. Creaven, B. Duff, D. A. Egan, K. Kavanagh, G. Rosair, V. R. Thangella, M. Walsh, *Inorg. Chim. Acta*., 2010, **363**, 4048.

14 (a) K. Nakamoto, Infrared and Raman Spectra of Inorganic and Coordination Compounds, Wiley, New York, 5th edn., 1997. (b) H. Fang-Hong, T. Lin, X. Li, Y. Li, Z. Wu and C. Yan, *New J. Chem*., 2012, **36**, 2078.

15 S. Zhu, F. Kou, H. Lin, C. Lin, M. Lin, and Y. Chen, *Inorg. Chem*., 1996, **35**, 585.

16 P. Ramadevi, R. Singh, A. Prajapati, S. Gupta, and D. Chakraborty, *Adv. Chem*., 2014, 14, 1.

17 M. S. Refat, I. M. El-Deen, H. K. Ibrahim and S. El-Ghoo; Spectrochim. *Acta. Part A Mol. Biomol. Spectrosc*., 2006, **65**, 1208.

18 (a) Y. Thio, X. Yang and J. J. Vittal, *Dalton Trans*., 2014, **43**, 3545. (b) S. Anbu, M. Kandaswamy, S. Kamalraj, J. Muthumarry and B. Varghes, *Dalton Trans*., 2011, **40**, 7310.

19 (a) L. Infantes, S. Motherwell, *CrystEngComm*., 2002, **4**, 454. (b) M. Mascal, L. Infantes, J. Chisholm, *Angew. Chem. Int. Ed*., 2006, **45**, 32 (c) L. Infantes, J. Chisholm and S. Motherwell, *CrystEngComm.*, 2003, **5**, 480. (d) W. Cao, Xiang-J. Zheng, De-C. Fang and Lin-P. Jin, *Dalton Trans*., 2014, **43**, 7298.

20 (a) W. Addison, T.N. Rao, J. Reedijk, J. Vm Riju, G.C. Verschoor, *J. Chem. Soc., Dalton Trans.*, 1984, 1349. (b) Codes- BIHWAR; CACLAV; FEFNOTO3; IFURIL; JAMNIV; LALVOK; PEKZAI; TISKIQ; YIRMUI; ZEGDUM

21 X. Pu, X. Zhang and Z. Li, *Acta Crystallogr*., 2008, **E64**, m216.

22 (a) R. K. Das, M. Sarkar, S. M. W. Rahaman, H. Doucet and J. K. Bera. *Eur. J. Inorg. Chem.* 2012, 1680. (b) H. S. Jena, *New J. Chem*., 2014, **38**, 2486.

23 A. F. Tanious, D.Y. Ding, D. A. Patrick, C. Bailly, R. R. Tidwell and W. D. Wilson, *Biochemistry*, 2002, **39**, 12091.

24 C. Y. Zhong, J. Zhao, Y. B. Wu, C. X. Yin and P. Yang, *J. Inorg. Biochem*., 2007, **101**, 10.

25 A. Wolf, G. H. Shimer and T. Meehan, *Biochemistry*, 1987, **26**, 6392.

26 F. J. M. Almes and D. Porschke, *Biochemistry*, 1993, **32**, 4246.

27 (a) Z. C. Liu, B. D. Wang, Z. Y. Yang, Y. Li, D. D. Qin and T. R. Li, *Eur. J. Med. Chem.,*2009, **44**, 4477. (b) C. Rajarajeswari, R. Loganathan, M. Palaniandavar, E. Suresh, A. Riyasdeen and M. A. Akbarsha, *Dalton Trans*., 2013, **42**, 8347.

28 (a) E. Ramachandran, D. S. Raja, N. S. P. Bhuvanesh and K. Natarajan, *Dalton Trans*., 2012, **41**, 13308. (b) D. S. Raja, N. S. P. Bhuvanesh and K. Natarajan, *Dalton Trans*., 2012, **41**, 4365 (c) D. S. Raja, N. S. P. Bhuvanesh and K. Natarajan, *Eur. J. Med. Chem.,* 2011, **46**, 4584. (d) R. Loganathan, S. Ramakrishnan, E. Suresh, M. Palaniandavar, A. Riyasdeen and M. A. Akbarsha, DaltonTrans., 2014, **43**, 6177.

29 V. G. Sankareswari, D. Vinod, A. Mahalakshmi, M. Alamelu, G. Kumaresan, R. Ramaraj and S. Rajagopal, *Dalton Trans*., 2014, **43**, 3260.

30 (a) J. N. Miller, *Proc. Anal. Div. Chem. Soc.,* 1979, **16**, 203. (b) J. H. Tang, F. Luan, X. G. Chen, *Bioorg*. *Med*. *Chem*., 2006, **49**, 3210.

31 M. A. Thompson, ArgusLb 4.0; Planaria Software LLC: Seattle, WA; http://www.arguslab.com

32 S. Tabassum, M. Zaki, M. Afzal and F. Arjmand, *Dalton Trans*., 2013, **42**, 10029.

33 A. Manna and S. Chakravorti, *Mol. BioSyst.,* 2013, **9**, 246.

35 H. H. Aung, S. R. Mehendale, C. Z. Wang, J. T. Xie, E. McEntee and C. S. Yuan, *Cancer Chemother. Pharmacol.*, 2007, **59**, 369S.

36 K. H. Jung, M. Choi, D. Y. Kim, H. S. Lee, H. Zheng, G. Y. Li, I. M. Deeb, B. S. Park, S. H. Lee and S. Hong, *Int. J. Oncology,* 2012, **41**, 1715.

37 (a) J. Shaoa, Z. Maa, A. Li, Y. H. Liu, C. Z. Xie, Z. Y. Qiang, J. Y. Xu, *J. Inorg. Biochem*., 2014, **136**, 13. (b) W. Guo, S. Ye, N. Cao, J. Huang, J. Gao, Q. Chen, *Exp. Toxicol. Pathol*., 2010, **62**, 577.

38 L. E. Bröker, F. A. Kruyt, G. Giaccone, *Clin. Cancer Res*., 2005, 11 3155.

Table 1 Crystal data and structure refinement parameters for **HL** and **CuL**

	HL	**CuL**
Empirical formula	$C_{21}H_{21}N_3O_3$	$C_{42}H_{32}Cu_2N_8O_8$
Crystal system	triclinic	monoclinic
Space group	*P*-1	$P2_1/n$
a (Å)	5.5526(11)	10.265(2)
b (Å)	10.809(2)	10.433(2)
c (Å)	16.095(3)	17.873(4)
α (deg)	93.298(10)	90.00
β (deg)	91.208(9)	94.202(11)
γ (deg)	98.123(10)	90.00
V (Å^3), *Z*	954.2(3)	1909.0(7)
λ (Å)	0.71073	0.71073
Colour and habit	Light yellow, needle	Green, block
T (K)	296(2)	296(2)
reflns collected	13905	15497
refins/restraint/params	3861/4/258	4267/0/271
D_{calcd} (Mg m^{-3})	1.265	1.572
μ (mm^{-1})	0.086	1.182
GOF on F^2	1.002	0.957
final *R* indices $I>2\sigma(I)$	R1 = 0.0530	R1 = 0.0476
	wR2 = 0.1257	wR2 = 0.0956
R indices (all data)	R1 = 0.1267	R1 = 0.1043
	R2 = 0.1633	wR2 = 0.1168